Title

Imipramine blue halts head and neck cancer invasion through promoting F-box and leucine-rich repeat protein 14-mediated Twist1 degradation

Permalink

https://escholarship.org/uc/item/6rv4m68r

Journal

Oncogene, 35(18)

ISSN

0950-9232

Authors

Yang, W-H
Su, Y-H
Hsu, W-H
et al.

Publication Date

2016-05-05

DOI

10.1038/onc.2015.291

Peer reviewed

Imipramine blue halts head and neck cancer invasion through promoting F-box and leucine-rich repeat protein 14-mediated Twist1 degradation

W-H Yang[1], **Y-H Su**[1], **W-H Hsu**[1], **C-C Wang**[2,3,4], **JL Arbiser**[5,6], and **M-H Yang**[1,7,8,9]

[1]Institute of Clinical Medicine, National Yang-Ming University, Taipei, Taiwan

[2]Department of Otolaryngology-Head & Neck Surgery, Taichung Veterans General Hospital, Taichung, Taiwan

[3]School of Medicine, National Yang-Ming University, Taipei, Taiwan

[4]School of Speech Language Pathology & Audiology, Chung-Shan Medical University, Taichung, Taiwan

[5]Department of Dermatology, Emory School of Medicine, Atlanta, GA, USA

[6]Atlanta Veterans Administration Medical Center, Atlanta, GA, USA

[7]Institute of Biotechnology in Medicine, National Yang-Ming University, Taipei, Taiwan

[8]Genome Research Center, National Yang-Ming University, Taipei, Taiwan

[9]Division of Hematology-Oncology, Department of Medicine, Taipei Veterans General Hospital, Taipei, Taiwan

Abstract

The unique characteristic of head and neck squamous cell carcinoma (HNSCC) is that local invasion rather than distant metastasis is the major route for dissemination. Therefore, targeting the locally invasive cancer cells is more important than preventing systemic metastasis in HNSCC and other invasive-predominant cancers. We previously demonstrate a specific mechanism for HNSCC local invasion: the epithelial–mesenchymal transition (EMT) regulator Twist1 represses microRNA let-7i expression, leading to the activation of the small GTPase Rac1 and engendering the mesenchymal-mode movement in three-dimensional (3D) culture. However, targeting the EMT regulator is relatively difficult because of its transcription factor nature and the strategy for confining HNSCC invasion to facilitate local treatment is limited. Imipramine blue (IB) is a newly identified anti-invasive compound that effectively inhibits glioma invasion. Here we demonstrate that in HNSCC cells, a noncytotoxic dose of IB represses mesenchymal-mode migration in two-

Correspondence: Professor JL Arbiser, Department of Dermatology, Winship Cancer Institute, Atlanta and Atlanta Veterans Administration Hospital, Emory University School of Medicine, WMB 5309, 1639 Pierce Drive, Atlanta, GA 30322, USA or Dr M-H Yang, Institute of Clinical Medicine, National Yang-Ming University, No. 155, Sec. 2, Li-Nong Street, Taipei 11221, Taiwan. jarbise@emory.edu or mhyang2@vghtpe.gov.tw.

and-a-half-dimensional/3D culture system. IB suppresses EMT and stemness of HNSCC cells through inhibition of Twist1-mediated let-7i downregulation and Rac1 activation and the EMT signalling. Mechanistically, IB inhibits reactive oxygen species-induced nuclear factor-κB pathway activation. Importantly, IB promotes degradation of the EMT inducer Twist1 by enhancing F-box and leucine-rich repeat protein 14 (FBXL14)-mediated polyubiquitination of Twist1. Together, this study demonstrates the potent anti-invasion and EMT-inhibition effect of IB, suggesting the potential of IB in treating local invasion-predominant cancers.

INTRODUCTION

Head and neck squamous cell carcinoma (HNSCC), which comprises tumours arising from oral cavity, oropharynx, hypopharynx and larynx, is one of the most devastating cancers worldwide.[1] A unique characteristic of HNSCC is that local invasion and regional lymph node involvement are the major causes of cancer mortality, and the incidence of distant organ metastasis is relatively rare in advanced disease compared with other cancers.[2] Standard treatments for advanced HNSCC therefore primarily aim to eradicate local–regional tumours, and chemoradiotherapy with or without surgery is the main strategy for locally advanced disease.[3–5] Unfortunately, local invasion makes the surgical eradication of advanced tumours difficult, and invasive HNSCC is likely to develop resistance to chemoradiotherapy.[3–5] Therefore, developing therapeutic strategies that specifically target the pathways responsible for local invasion is extremely important in improving the treatment outcome of advanced HNSCC.

The migration behaviour of cancer cells in three-dimensional (3D) environments reflects the clinical characteristics of cancer dissemination.[6] Individual cancer cells move either in a mesenchymal mode or in an amoeboid mode. The mesenchymal mode is characterized by the elongated shape of tumour cells with pseudopods, whereas the amoeboid movement is hallmarked by round-shaped cancer cells with intensive membranous blebbing.[7–9] Recent studies have suggested that the mesenchymal-mode movement is responsible for the local invasion of tumour cells; in contrast, amoeboid migration correlates with distant metastasis.[10–11] Our recent findings provide the mechanistic link between individual cell movement and the epithelial–mesenchymal transition (EMT), a major mechanism of cancer metastasis.[12–14] We demonstrate that the EMT inducer Twist1 represses the expression of the microRNA let-7i, resulting in the upregulation of NEDD9 and DOCK3, which are the co-activators of the small GTPase Rac1, and the morphogenic protein BMP4. The mesenchymal-mode movement is therefore engendered and plays a critical role in the local invasion of HNSCC.[15,16] Therefore, targeting HNSCC local invasion may be feasible by suppressing the signal pathways identified as involved in cancer invasiveness.

In recent years, an increasing number of investigations toward the development of anti-invasive compounds have led to the discovery of promising agents against migratory cancer cells.[17,18] Notably, considerable attention was directed towards the development of an anti-invasive agent targeting glioblastoma because it is a devastating tumour with highly invasive behaviour but seldom metastasizes to extracranial tissues.[19,20] Recently, imipramine blue (IB), an organic triphenylmethane blue dye that is the derivative of the antidepressant drug

imipramine, has been shown to effectively repress glioma cell invasion in a highly aggressive RT2 syngeneic astrocytoma rodent model. Mechanistically, IB inhibits NADPH (the reduced form of nicotinamide adenine dinlucleotide phosphate) oxidase 4 activity to attenuate the production of reactive oxygen species (ROS). IB also modulates the expression of cytoskeleton regulatory genes, resulting in the disruption of actin fibre formation. Furthermore, IB demonstrates synergy with the chemotherapeutic agent doxorubicin in treating glioblastoma.[18] In this study, we investigated the effectiveness of IB as an anti-invasive agent for HNSCC owing to the overlapping phenotypes between IB-treated glioma cells and noninvasive HNSCC cells in our previous studies. We demonstrate that IB harbours potent anti-invasive effects in suppressing HNSCC invasion by disrupting Twist1- and nuclear factor-κB (NF-κB)-mediated pathways.

RESULTS

IB treatment suppresses mesenchymal-mode movement and local invasion of HNSCC

Because IB has been shown to be an effective anti-invasive agent in suppressing glioma invasion,[18] and local invasion is the major mode of HNSCC progression,[2,3] we initiated this study to investigate the anti-invasive effect of IB in HNSCC. First, we determined the cytotoxic effect of IB (Figure 1a) in four HNSCC cell lines (OECM-1, SAS, CAL-27 and FaDu) and a primary HNSCC culture (Supplementary Figure S1a and Supplementary Table S1). Our previous study showed that the doses of IB with anti-invasive effects are below the cytotoxic levels in glioma cells.[18] To investigate the anti-invasive effect of IB, we selected a subcytotoxic dose of IB (1 μM for 24 h) for treating HNSCC cells in subsequent experiments. Because the 3D cultivation system represents the living microenvironment and is superior to traditional culture systems for studying cancer cell migration[21,22] and mesenchymal-mode movement in 3D culture is critical for HNSCC invasion,[15] we used the two-and-a-half-dimensional (2.5D) culture system (where cells are plated on top of thick collagen) to investigate the effect of IB on HNSCC movement (Figure 1b). The invasiveness of HNSCC cell lines has been characterized previously: OECM-1 and SAS are highly invasive cell lines, whereas FaDu cells exhibit a relatively lower invasive capability.[15] The results indicated that treatment of OECM-1 cells with IB resulted in a rounded shape as evidenced by the changes in 3D-reconstructed immunofluorescent image (Figure 1c) and morphology index (Figure 1d). A similar effect of IB in changing the morphology index was demonstrated in another highly invasive HNSCC cell line, SAS, and a primary HNSCC culture (Figure 1e). Furthermore, IB reduced the motility of OECM-1 cells in 2.5D culture in a dose-dependent manner (Figure 1f). Treatment of OECM-1 with IB reduced invasiveness in the 3D culture system (Figure 1g). To confirm the anti-invasive effect of IB on HNSCC *in vivo*, we inoculated SAS cells into the tongue of nude mice. After formation of the orthotopic tumours, we treated the mice with IB or a control vehicle for 3 weeks and then killed the mice for histological examination of the xenotransplanted tumours. The results showed that in the IB treatment group, a well-defined border was present between the tumours and the adjacent muscular tissues. In contrast, a prominent muscular invasion of the tumours was demonstrated in the mice without IB treatment (Figure 1h). Considering the effect of IB on tumour size, we measured the bioluminescent intensity of the SAS-derived orthotopic tumours with or without IB treatment. Here, IB showed a modest effect in suppressing

tumour growth (Supplementary Figures S1b and c). Together, these results indicate that the noncytotoxic dose of IB treatment suppressed the mesenchymal-mode movement of HNSCC cells and abrogated the local invasion of xenotransplanted tumours in *vivo*.

IB treatment inhibits Twist1-induced EMT and mesenchymal movement

Because Twist1-mediated Rac1 activation is responsible for the mesenchymal movement and invasiveness of HNSCC,[15] we examined the impact of IB on Twist1-induced EMT and mesenchymal migration. The result showed that IB repressed Twist1 expression and reversed EMT as evidenced by increasing the expression of epithelial markers (E-cadherin and γ-catenin) and decreasing the mesenchymal marker N-cadherin in a dose-dependent manner in both OECM-1 cells (Figure 2a) and a primary HNSCC culture (Supplementary Figure S2a). A subcytotoxic dose of IB (1 μM) also reduced Twist1 and reversed the EMT phenotype in SAS cells (Supplementary Figure S2b). Morphologically, IB increased the expression of intercellular E-cadherin and reduced cytoplasmic vimentin levels in OECM-1 cells (Figure 2b). Because Twist1 engenders mesenchymal-mode movement by repressing let-7i to induce the expression of Rac1 co-activators NEDD9 and DOCK3,[15] we examined the level of let-7i, NEDD9, DOCK3 and GTP-bound Rac1 in OECM-1 cells treated with IB. IB upregulated let-7i expression (Figure 2c) and correspondingly reduced NEDD9 and DOCK3 expression, leading to Rac1 inactivation (Figure 2d). Consistently, IB treatment in FaDu-Twist1 transfectants reversed Twist1-induced EMT (morphological reversion, reduced N-cadherin expression and increased E-cadherin expression) and suppressed DOCK3 and NEDD9 expression (Figures 2e and f). In FaDu cells, IB treatment abrogated Twist1-induced mesenchymal morphology and motility in 2.5D culture (Figures 2g and h). IB also mitigated Twist1-induced invasiveness in 3D environments (Figure 2i). These data suggest that IB abrogates Twist1-induced EMT and mesenchymal migration in HNSCC cells.

IB treatment reduces stem-like properties of HNSCC cells

As Twist1-induced EMT promotes cancer stemness[23,24] and IB reverses Twist1-induced EMT in HNSCC, we next examined whether IB treatment could repress stem-like properties in HNSCC. The result showed that ectopic expression of Twist1 in FaDu cells enhanced the sphere-forming capability, as expected. A subcytotoxic dose of IB treatment in FaDu-Twist1 cells reduced the sphere formation ability back to levels similar to FaDu-control cells. The size of formed spheres was also reduced by IB (Figure 3a). IB treatment also inhibited the sphere-forming ability and the sphere diameter of primary HNSCC cells (Figure 3b). Furthermore, IB treatment suppressed the anchorage-independent growth of the highly invasive OECM-1 cells and primary HNSCC cells (Figure 3c). The proportion of CD44-positive cells, which is a marker of HNSCC stem cells,[25] in both OECM-1 and SAS cells was also significantly reduced after IB treatment (Figure 3d). These results suggest that in addition to the effect of inhibiting mesenchymal migration and EMT, IB also reduces the stem-like properties of HNSCC cells.

IB inactivates the NF-κB pathway

Next, we investigated the mechanism of IB-induced downregulation of Twist1 expression. We previously showed that IB represses the activity of NADPH oxidase 4 to reduce the production of ROS[18] that has been shown to be an important factor for inducing NF-κB

activation.[26] Furthermore, NF-κB activates the transcription of *TWIST1* to induce EMT.[27] We therefore hypothesized that IB inhibits Twist1 expression through inactivating the NF-κB pathway. We first examined whether IB treatment reduces ROS production in HNSCC cells. The results showed that IB treatment in OECM-1 cells reduced ROS production (Figure 4a). Importantly, IB treatment efficiently blocked the nuclear translocation of p65 in two highly invasive HNSCC cell lines, OECM-1 and SAS (Figure 4b). Electrophoretic mobility shift assays showed that IB markedly reduced NF-κB binding activity in the nuclear extracts from OECM-1 cells (Figure 4c). A NF-κB reporter assay showed that treatment of hydrogen peroxide increased the reporter activity, and IB treatment attenuated the ROS-induced reporter activation (Figure 4d). To confirm the suppression of NF-κB pathway by IB in HNSCC cells, we examined the expression levels of two NF-κB target genes, *IL1B*[28] and *IL6*,[29] in IB-treated HNSCC cells compared with untreated cells. Consistently, hydrogen peroxide upregulated the expression of these target genes and treatment of IB inhibited the ROS-induced target genes expression in OECM-1 cells (Figure 4e). Because NF-κB induces Twist1 expression through the transcriptional activation of *TWIST1*,[27] we examined whether IB treatment could decrease *TWIST1* mRNA levels. Surprisingly, *TWIST1* mRNA levels were not significantly changed by IB treatment in OECM-1, SAS and primary HNSCC cells (Supplementary Figure S3). Taken together, these results suggest that IB reduces ROS generation and inactivates NF-κB signalling. However, *TWIST1* transcription was not influenced by IB, suggesting the involvement of other mechanisms in regulating Twist1 expression under IB treatment.

IB promotes Twist1 degradation through FBXL14-mediated polyubiquitination

Because IB treatment did not significantly reduce *TWIST1* transcription, we examined whether IB could affect the stability of Twist1 protein. A cycloheximide pulse-chase assay showed that IB reduced Twist1 stability in OECM-1 cells (Figure 5a). The stability of Twist1 in FaDu-Twist1 transfectants was also reduced by IB (Supplementary Figure S4a). Because polyubiquitination is a major mechanism for protein degradation by proteasomes,[30] we added the proteasome inhibitor MG132 to IB-treated SAS cells and observed whether the IB-mediated Twist1 degradation could be rescued by the proteasome inhibitor. The result showed that MG132 treatment prevented IB-mediated Twist1 degradation (Figure 5b). Furthermore, the addition of IB to Twist1-transfected 293T cells markedly increased Twist1 polyubiquitination (Figure 5c), suggesting that IB promotes Twist1 degradation through enhancing polyubiquitination-mediated proteasome degradation. Next, we aimed to elucidate the E3 ligase responsible for IB-mediated Twist1 degradation. Previous studies have found that two E3 ligases, FBXL14 and β-Trcp, are involved in the proteasome-dependent Twist1 degradation.[31,32] Immunoprecipitation experiments showed that IB enhanced the interaction between Twist1 and FBXL14 but not β-Trcp (Figure 5d). A proximity ligation assay (PLA) further confirmed the enhancement of the Twist1-FBXL14 interaction by IB (Figures 5e and f). Furthermore, deletion of the F-box in FBXL14, indicating the loss of binding capability of FBLX14 to the SKP1-cullin 1-F-box protein (SCF) E3 ligase complex,[33] abrogated FBXL14-mediated Twist1 polyubiquitination (Figure 5g).

Next, we elucidated whether IB also affects the stability of other proteins in the Twist1-let-7i-NEDD9 pathway and EMT. The result showed that IB did not change the stability of NEDD9, a downstream target of the Twist1-let-7i pathway[15] that mediates mesenchymal movement (Supplementary Figure S4b). Interestingly, IB reduced the expression of other EMT regulators, including Zeb1, Zeb2, Snail and Slug, in HNSCC cell lines and primary cultures (Supplementary Figure S4c). Collectively, these data suggest that IB promotes Twist1 degradation through enhancing the interaction between Twist1 and the E3 ligase FBXL14 that induces the polyubiquitination of Twist1 to undergo proteasome degradation. For regulating the Twist1-mediated pathway, IB specifically promotes Twist1 degradation without affecting the stability of the downstream target NEDD9. In addition to promoting Twist1 degradation, IB also repressed the expression of other EMT regulators (Zeb1, Zeb2, Snail and Slug) in HNSCC cells.

IB treatment inhibits Twist1-induced tumour invasion and metastatic colonization *in vivo*

Finally, we confirmed the effect of IB in attenuating Twist1-induced local invasion *in vivo*. We first investigated the effect of IB on xenotransplanted tumour growth and invasion. The FaDu-Twist1 and FaDu-control transfectants were inoculated in the subcutaneous region of the nude mice. After the formation of xenografted tumours, IB was administered through intravenous injection consecutively for 6 weeks. The mice were killed for the measurement of tumour volumes and the histologic examination of tumour invasion (Figure 6a). The result showed that IB treatment reduced tumour volume (Figure 6b). Importantly, IB abrogated Twist1-induced invasion. In FaDu-control cell tumours, a distinct border between the tumours and the adjacent muscles were noted; in contrast, FaDu-Twist1 tumours demonstrated a prominent muscular invasion. IB treatment in mice receiving FaDu-Twist1 inoculation resulted in the reconstitution of the tumour-muscle boundary in xenografted tumours (Figure 6c). We next investigated whether IB affects metastatic colonization because IB reduces cancer stemness, an important characteristic for colonizing metastatic tumours. FaDu-Twist1 and FaDu-control cells were intravenously injected into the mice, and IB was delivered weekly immediately after tumour cell injection. The mice were killed after 8 weeks for examination of metastatic tumours (Figure 6d). The results showed that FaDu-Twist1 had a significantly higher capability of forming metastatic lung tumours and that IB treatment effectively repressed the development of metastatic tumours (Figure 6e). We propose a model for summarizing our findings in Figure 6f. In invasive HNSCC, the NF-κB pathway and Twist1 promote EMT, mesenchymal movement and cancer stemness, leading to local tumour progression. IB treatment inhibits NADPH oxidase 4 activity, resulting in the reduction of ROS generation and NF-κB pathway inactivation. Furthermore, IB promotes Twist1 interacts with FBXL14 to induce Twist1 degradation. Blockage of these two pathways abrogates local HNSCC invasion, suggesting the anti-invasive effect of IB in HNSCC.

DISCUSSION

Different types of cancers disseminate in distinct manners according to their unique biological characteristics. For example, melanoma and breast cancer frequently metastasize to distal organs, and ovarian cancer typically directly implants into the peritoneal tissues.

HNSCC and brain tumours preferentially invade into the adjacent tissues. Customizing the therapeutic strategy based on the disseminating routes should improve the treatment outcome of different cancers. For invasion-predominant cancers, local infiltration results in a less-defined tumour margin that reduces the success rate of surgical eradication or radiation. Furthermore, the invasive cancer cells are usually more resistant to cytotoxic agents than the confined cancer cells. However, most anticancer treatments are cytotoxic, and the available anti-invasive compounds are very limited. Therefore, development of anti-invasive agents to halt cancer movement is critically important for improving the treatment outcome of invasion-predominant cancers. In this study, we demonstrate that IB prevents HNSCC cell invasion. The *in vivo* data suggest that IB not only inhibits HNSCC invasion but also harbours a moderate antiproliferative activity against HNSCC. The possible explanation is that IB suppresses the activity of several crucial pathways for cellular proliferation and survival, such as NF-κB (confirmed in this study), phosphatidylinositol 3-kinase/Akt and protein kinase C pathway.[18] Together with our previous finding in glioma,[18] we suggest that IB is an effective anti-invasive compound in treating invasive-predominant cancers. Further studies to investigate the synergy of combining IB with other cytotoxic agents or molecular targeting agents will be necessary.

Our previous study has demonstrated the major anti-invasive mechanisms of IB, including the inhibition of NADPH oxidase 4 to reduce ROS generation and alterations of actin fibre formation.[18] However, how the suppression of NADPH oxidase 4 could repress tumour invasion and the mechanism of how IB influences actin fibre formation remained unclear. In this study, we elucidated two antitumour mechanisms of IB, including the inactivation of the NF-κB pathway and the promotion of Twist1 degradation. We first demonstrate that IB reduces ROS generation and inactivates NF-κB signal pathway. Intriguingly, although NF-κB has been shown to induce *TWIST1* transactivation,[27] we found that IB prevents Twist1 signalling by promoting Twist1 degradation rather than inhibiting transcription. The importance of blocking Twist1 signal in the prevention of local invasion is that, in addition to being an EMT inducer, Twist1 plays a major role in regulating local invasion through Rac1 activation to engender mesenchymal-mode movement.[15] The dual anti-invasive effects highlight the unique role of IB in treating invasive cancers.

Here, we found that IB promotes the interaction between Twist1 and FBXL14 to induce Twist1 degradation. A previous study demonstrates that Ppa, the Xenopus homologue of FBXL14, promotes polyubiquitination and degradation of the EMT regulators Twist, Snail, Slug and SIP1.[30] Furthermore, FBXL14 causes Snail degradation in hypoxic environments.[34] These findings indicate that the stability of different EMT regulators is controlled in a concerted manner by the E3 ligase at a higher hierarchical level. Interestingly, we also showed that IB reduces the expression of other EMT regulators (Snail, Slug, Zeb1 and Zeb2) in addition to destabilizing Twist1 in HNSCC cells. Because EMT is one of the major mechanisms for cancer invasion,[12,13] and targeting EMT factors is relatively difficult owing to their transcription factor nature, our study may indicate an important strategy for disrupting EMT in human cancers that has not previously been addressed. However, further studies to elucidate whether IB suppresses the expression of other EMT regulators in a similar mechanism, that is, enhancement of the interaction between FBXL14 and other EMT

factors to promote their degradation and to determine the specificity of IB in targeting mesenchymal-like cancer cells, is mandatory.

Although most data support the fact that IB mainly acts as an anti-invasive agent, and here we showed that a noncytotoxic dose of IB is also able to reduce stem-like properties *in vitro*, and IB inhibits metastatic colonization *in vivo*. The possible explanation is that EMT is critical not only in cancer invasion but also in the generation of stem-like properties of cancer cells.[13,23,24] IB suppresses the expression of Twist1 and other EMT regulators, suggesting that IB is a potent EMT inhibitor. The metastatic inhibition effect by IB is attributed to the suppression of cancer stemness rather than direct cytotoxicity.

In conclusion, our findings have elucidated the anti-invasive mechanisms of IB in HNSCC cells, highlighting the unique role of IB in treating invasion-predominant cancers. Importantly, the potential of IB as a potent EMT inhibitor has emerged in this study. According to the previous studies and the current finding, combinatory treatment by incorporating bulky-tumour eradication therapy (cytotoxic therapy/target therapy), anti-invasive therapy and microenvironment-modulating therapy (antiangiogenic/tumour immunotherapy) will be an attractive strategy for managing advanced cancers in the future.

MATERIALS AND METHODS

Cell lines and plasmids

Two human head and neck cancer cell lines (FaDu and CAL-27), the human embryonic kidney cell line 293T and the mouse embryo fibroblast cell line NIH3T3 were originally obtained from ATCC (Manassas, VA, USA). The human head and neck cancer cell line SAS and the human umbilical vein endothelial cells were purchased from Bioresource Collection and Research Center of Taiwan (Hsinchu City, Taiwan). The human head and neck cancer cell line OECM-1 was kindly provided by Dr Kuo-Wei Chang (National Yang-Ming University, Taipei, Taiwan). The cell lines were not authenticated recently, and they had been confirmed without mycoplasma contamination. The expression vectors pcDNA3-myc-FBXL14 and pcDNA3-FBXL14 F were gifts from Professor Víctor M Díaz (Universitat Pompeu Fabra, Barcelona, Spain). pCDH-Twist1 was generated by inserting full-length complementary DNA (NM_000474.3) into pCDH-CMV-MCS-EF1-puro.

IB treatment of HNSCC cells

The HNSCC cell lines received the treatment of IB as indicated doses for 24 h and then were subjected to subsequent experiments and analyses. The assays include MTT assay, 2.5D culture and morphology analysis, speed quantification, 3D invasion assay, spheroid formation assay, soft agar assay, flow cytometry, analysis of the target molecules by western blot or quantitative PCR, ROS detection assay, electrophoretic mobility shift assay, reporter assay, proximity ligation assay and immunoprecipitation.

Cell viability assay and calculation of half-maximal inhibitory concentration value

A total of 5×10^4 cells per well were seeded in a 96-well plate with triplicate and incubated for 24 h and then treated with different concentrations of IB. After 24 h of treatment, the

medium was removed. The MTT assay solution was added to each well, and the plate was incubated for 1 h at 37 °C. After incubation, the solution was carefully discarded and dimethyl sulphoxide was added to dissolve newly formed mitochondrial MTT crystals. Finally, the plate was read using a microplate reader at 540 nm. Based on the data of cell viability assay, half-maximal inhibitory concentration value calculation was performed by Sigmaplot 10.0 (Systat Software Inc., San Jose, CA, USA).

DCFDA cellular ROS detection assay

A DCFDA cellular ROS detection assay (Abcam PLC, Cambridge, MA, USA) was used to measure hydroxyl, peroxyl and other ROS activity within the cell. A total of 2.5×10^4 cells per well were seeded on a 96-well plate and allowed to attach for 16 h. The cells were then stained with 25 μM DCFDA for 45 min at 37 °C. After staining, the cells were treated with 1 μM IB for 6 h. Finally, the fluorescent intensity was determined by fluorescence spectroscopy with maximum excitation and emission spectra of 495 and 529 nm, respectively.

Electrophoretic mobility shift assay

The DNA binding amount of NF-κB was determined using the NF-κB electrophoretic mobility shift assay kit (No. GS0030, Signosis, Inc., Santa Clara, CA, USA). Briefly, a biotin-labelled DNA probe containing specific binding sequence of NF-κB was incubated with the nuclear extracts from OECM-1 cells treated with IB or the NF-κB inhibitor parthenolide. Electrophoresis was performed, and the gel was transferred to a nylon membrane. NF-κB binding to the probe was detected by strepatvidin–horseradish peroxidase and a chemiluminescent substrate. In the competition assay, excess amounts of unlabelled competitors were added before the labelled probes. The concentration of the probe was 20 ng/μl.

Proximity ligation assay

The PLA was used to investigate the proximity of epitopes recognized by the anti-Twist1 and anti-FBXL14 antibodies that represent the association of Twist1 with FBXL14 in cancer cells. The experiment and data analysis was performed as previously described.[35] The data are presented as the presence of the PLA signal per cell and the percentage of PLA signal-positive cells. Costaining of anti-Twist1 and anti-Bmi1 was used as a positive control for the experiment because the interaction between Twist1 and Bmi1 has been demonstrated in HNSCC cells.[23] Staining with anti-FBXL14 alone was performed as a negative control.

Reverse transcription and quantitative PCR

The experiment was performed as described previously.[15] The primer sequences were as follows: let-7i stem-loop RT primer, 5′-GTCGTATCC AGTGCAGGGTCCGAGGTATTCGCACTGGATACGACAACAGC-3′; PCR primers, let-7i forward 5′-GCCGCTTGAGGTAGTAGTTTGT-3′ and reverse 5′-GTGCAG GGTCCGAGGT-3′; U6 forward 5′-CTCGCTTCGGCAGCAC-3′ and reverse 5′-AACGCTTCACGAATTTGCG-3′; *GAPDH* forward 5′-AAGGTCGGAGTCAA CGGATTTG-3′ and reverse 5′-CCATGGGTGGAATCATATTGGAA-3′; *IL1B* forward 5′-

AAGCCCTTGCTGTAGTGGTG-3′ and reverse 5′-GAAGCTGATGGC CCTAAACA-3′; *IL6* forward 5′-GTCAGGGGTGGTTATTGCAT-3′ and reverse 5′-AGTGAGGAACAAGCCAGAGC-3′.

Rac1 pull down, immunoprecipitation and western blot analysis

The experiments were performed as described previously.[15,35] The primary antibodies used in the current study are listed in Supplementary Table S2.

Animal experiments

All experiments were performed according to the institutional animal welfare guidelines of the Taipei Veteran General Hospital. The animal experiments were in compliance with the ethical regulations and approved by the institutional animal care and utilization committee of Taipei Veterans General Hospital. There are three different animal experiments in this study, including orthotopic implantation assay for examining tumour invasiveness, subcutaneous implantation assay for measuring tumour volume and invasion and tail vein injection assay for detecting the metastatic colonization ability. For orthotopic implantation assay, 1×10^6 of SAS cells were injected in the tongue of 6-week-old female BALB/C nude mice ($n = 5$ mice per group). After formation of orthotopic tumours (10 days after tumour cells injection), IB 2 mg/kg was given intravenously twice a week for consecutive 3 weeks. Then, the mice were killed, and the tumours along with the adjacent tongues were harvested, fixed and embedded in paraffin. The paraffin-embedded tissues were stained with haematoxylin and eosin, and the invasive characteristic of the tumours was evaluated by microscopic examination. The experimental procedure is shown in the upper panel of Figure 1h. For the subcutaneous implantation assay, 1×10^6 of FaDu-CDH or FaDu-Twist1 cells were inoculated into the subcutaneous region of 6-week-old female BALB/C nude mice ($n = 5$ mice per group). IB 2 mg/kg was given intravenously once the implanted tumour volume reached 150mm^3. The mice were killed 6 weeks after IB treatment. The tumour volumes were measured and tumour invasiveness was examined microscopically. The experimental procedure and the representative images for xenotransplantation are shown in Figure 6a. For the tail vein injection assay, 6-week-old female NOD-SCID mice received injections of 1×10^6 of FaDu-CDH or FaDu-Twist1 cells in 0.1 ml of PBS through the tail vein ($n = 6$ mice per group). IB 2 mg/kg was given intravenously once a week for 8 consecutive weeks since the day of tumour cell injection. The mice were killed 8 weeks after tumour cell injection, and the metastatic nodules in lungs were quantified. The experimental procedure is illustrated in Figure 6d.

Statistical analysis

The numerical results are presented as mean ± s.e.m. No statistical method was used to predetermine sample size. The experiments were not randomized, and the investigators were not blinded to allocation during experiments and outcome assessment. Samples whose values were >2 s.d. from the mean were considered outliers and excluded from the analysis. Two-tailed independent Student's *t*-test was used to compare the continuous variables between two groups. The χ^2 test was applied to compare the dichotomous variables. All statistical data were derived from at least two biological independent experiments, and each

experiment contained two technical replicates. The level of statistical significance was set at $P < 0.05$ for all tests.

Experimental procedures

The experimental procedures such as culturing HNSCC cells on top of a thick layer of collagen (2.5D culture), analysis of cell morphology, quantification of motility speed by time-lapse microscopy, immunofluorescent staining and 3D image reconstruction, 3D invasion assay; flow cytometry, spheroid formation assay and soft agar colony formation assay are described in detail in the Supplementary Materials and methods. The experimental detail for 2.5D culture is provided in Supplementary Table S2.

Supplementary Material

Refer to Web version on PubMed Central for supplementary material.

Acknowledgments

References

1. Jemal A, Siegel R, Xu J, Ward E. Cancer statistics, 2010. CA Cancer J Clin. 2010; 60:277–300. [PubMed: 20610543]

2. Garavello W, Ciardo A, Spreafico R, Gaini RM. Risk factors for distant metastases in head and neck squamous cell carcinoma. Arch Otolaryngol Head Neck Surg. 2006; 132:762–766. [PubMed: 16847186]

3. Pentenero M, Gandolfo S, Carrozzo M. Importance of tumor thickness and depth of invasion in nodal involvement and prognosis of oral squamous cell carcinoma: a review of the literature. Head Neck. 2005; 27:1080–1091. [PubMed: 16240329]

4. Forastiere AA, Zhang Q, Weber RS, Maor MH, Goepfert H, Pajak TF, et al. Long-term results of RTOG 91-11: a comparison of three nonsurgical treatment strategies to preserve the larynx in patients with locally advanced larynx cancer. J Clin Oncol. 2013; 31:845–852. [PubMed: 23182993]

5. Lorch JH, Goloubeva O, Haddad RI, Cullen K, Sarlis N, Tishler R, et al. Induction chemotherapy with cisplatin and fluorouracil alone or in combination with docetaxel in locally advanced squamous-cell cancer of the head and neck: long-term results of the TAX 324 randomised phase 3 trial. Lancet Oncol. 2011; 12:153–159. [PubMed: 21233014]

6. Friedl P. Prespecification and plasticity: shifting mechanisms of cell migration. Curr Opin Cell Biol. 2004; 16:14–23. [PubMed: 15037300]

7. Sanz-Moreno V, Gadea G, Ahn J, Paterson H, Marra P, Pinner S, et al. Rac activation and inactivation control plasticity of tumor cell movement. Cell. 2008; 135:510–523. [PubMed: 18984162]

8. Sanz-Moreno V, Marshall CJ. The plasticity of cytoskeletal dynamics underlying neoplastic cell migration. Curr Opin Cell Biol. 2010; 22:690–696. [PubMed: 20829016]

9. Wyckoff JB, Pinner SE, Gschmeissner S, Condeelis JS, Sahai E. ROCK- and myosin-dependent matrix deformation enables protease-independent tumor-cell invasion in vivo. Curr Biol. 2006; 16:1515–1523. [PubMed: 16890527]

10. Panková K, Rösel D, Novotný M, Brábek J. The molecular mechanisms of transition between mesenchymal and amoeboid invasiveness in tumor cells. Cell Mol Life Sci. 2010; 67:63–71. [PubMed: 19707854]

11. Madsen CD, Sahai E. Cancer dissemination-lessons from leukocytes. Dev Cell. 2010; 19:13–26. [PubMed: 20643347]

12. Thiery JP, Acloque H, Huang RY, Nieto MA. Epithelial-mesenchymal transitions in development and disease. Cell. 2009; 139:871–890. [PubMed: 19945376]

13. Nieto MA. Epithelial plasticity: a common theme in embryonic and cancer cells. Science. 2013; 342:1234850. [PubMed: 24202173]

14. Tsai JH, Yang J. Epithelial-mesenchymal plasticity in carcinoma metastasis. Genes Dev. 2013; 27:2192–2206. [PubMed: 24142872]

15. Yang WH, Lan HY, Huang CH, Tai SK, Tzeng CH, Kao SY, et al. RAC1 activation mediates Twist1-induced cancer cell migration. Nat Cell Biol. 2012; 14:366–374. [PubMed: 22407364]

16. Yang WH, Lan HY, Tai SK, Yang MH. Repression of bone morphogenetic protein 4 by let-7i attenuates mesenchymal migration of head and neck cancer cells. Biochem Biophys Res Commun. 2013; 433:24–30. [PubMed: 23454123]

17. Di C, Mattox AK, Harward S, Adamson C. Emerging therapeutic targets and agents for glioblastoma migrating cells. Anticancer Agents Med Chem. 2010; 10:543–555. [PubMed: 20950259]

18. Munson JM, Fried L, Rowson SA, Bonner MY, Karumbaiah L, Diaz B, et al. Anti-invasive adjuvant therapy with imipramine blue enhances chemotherapeutic efficacy against glioma. Sci Transl Med. 2012; 4:127ra36.

19. Carlsson SK, Brothers SP, Wahlestedt C. Emerging treatment strategies for glioblastoma multiforme. EMBO Mol Med. 2014; 6:1359–1370. [PubMed: 25312641]

20. Newton HB, Rosenblum MK, Walker RW. Extraneural metastases of infratentorial glioblastoma multiforme to the peritoneal cavity. Cancer. 1992; 69:2149–2153. [PubMed: 1311985]

21. Evan-Ram S, Yamada KM. Cell migration in 3D matrix. Curr Opin Cell Biol. 2005; 17:524–532. [PubMed: 16112853]

22. Slorach EM, Chou J, Werb Z. Zeppo1 is a metastasis promoter that represses E-cadherin expression and regulates p120-catenin isoform expression and localization. Genes Dev. 2011; 25:471–484. [PubMed: 21317240]

23. Yang MH, Hsu DS, Wang HW, Wang HJ, Lan HY, Yang WH, et al. Bmi1 is essential in Twist1-induced epithelial- mesenchymal transition. Nat Cell Biol. 2010; 12:982–992. [PubMed: 20818389]

24. Mani SA, Guo W, Liao MJ, Eaton EN, Ayyanan A, Zhou AY, et al. The epithelial-mesenchymal transition generates cells with properties of stem cells. Cell. 2008; 133:704–715. [PubMed: 18485877]

25. Prince ME, Sivanandan R, Kaczorowski A, Wolf GT, Kaplan MJ, Dalerba P, et al. Identification of a subpopulation of cells with cancer stem cell properties in head and neck squamous cell carcinoma. Proc Natl Acad Sci USA. 2007; 104:973–978. [PubMed: 17210912]

26. Morgan MJ, Liu ZG. Crosstalk of reactive oxygen species and NF-κB signaling. Cell Res. 2011; 21:103–115. [PubMed: 21187859]

27. Li CW, Xia W, Huo L, Lim SO, Wu Y, Hsu JL, et al. Epithelial-mesenchymal transition induced by TNF-α requires NF-κB-mediated transcriptional upregulation of Twist1. Cancer Res. 2012; 72:1290–1300. [PubMed: 22253230]

28. Cogswell JP, Godlevski MM, Wisely GB, Clay WC, Leesnitzer LM, Ways JP, et al. NF-kappa B regulates IL-1 beta transcription through a consensus NF-kappa B binding site and a nonconsensus CRE-like site. J Immunol. 1994; 153:712–723. [PubMed: 8021507]

29. Libermann TA, Baltimore D. Activation of interleukin-6 gene expression through the NF-KB transcription factor. Mol Cell Biol. 1990; 10:2327–2334. [PubMed: 2183031]

30. Ravid T, Hochstrasser M. Diversity of degradation signals in the ubiquitin–proteasome system. Nat Rev Mol Cell Biol. 2008; 9:679–689. [PubMed: 18698327]

31. Lander R, Nordin K, LaBonne C. The F-box protein Ppa is a common regulator of core EMT factors Twist, Snail, Slug, and Sip1. J Cell Biol. 2011; 194:17–25. [PubMed: 21727196]

32. Zhong J, Ogura K, Wang Z, Inuzuka H. Degradation of the transcription factor Twist, an oncoprotein that promotes cancer metastasis. Discov Med. 2013; 15:7–15. [PubMed: 23375009]

33. Ho MS, Tsai PI, Chien CT. F-box proteins: the key to protein degradation. J Biomed Sci. 2006; 13:181–191. [PubMed: 16463014]

34. Viñas-Castells R, Beltran M, Valls G, Gómez I, García JM, Montserrat-Sentís B, et al. The hypoxia-controlled FBXL14 ubiquitin ligase targets SNAIL1 for proteasome degradation. J Biol Chem. 2010; 285:3794–3805. [PubMed: 19955572]

35. Hsu DS, Wang HJ, Tai SK, Chou CH, Hsieh CH, Chiu PH, et al. Acetylation of Snail modulates the cytokinome of cancer cells to enhance the recruitment of macrophages. Cancer Cell. 2014; 26:534–548. [PubMed: 25314079]
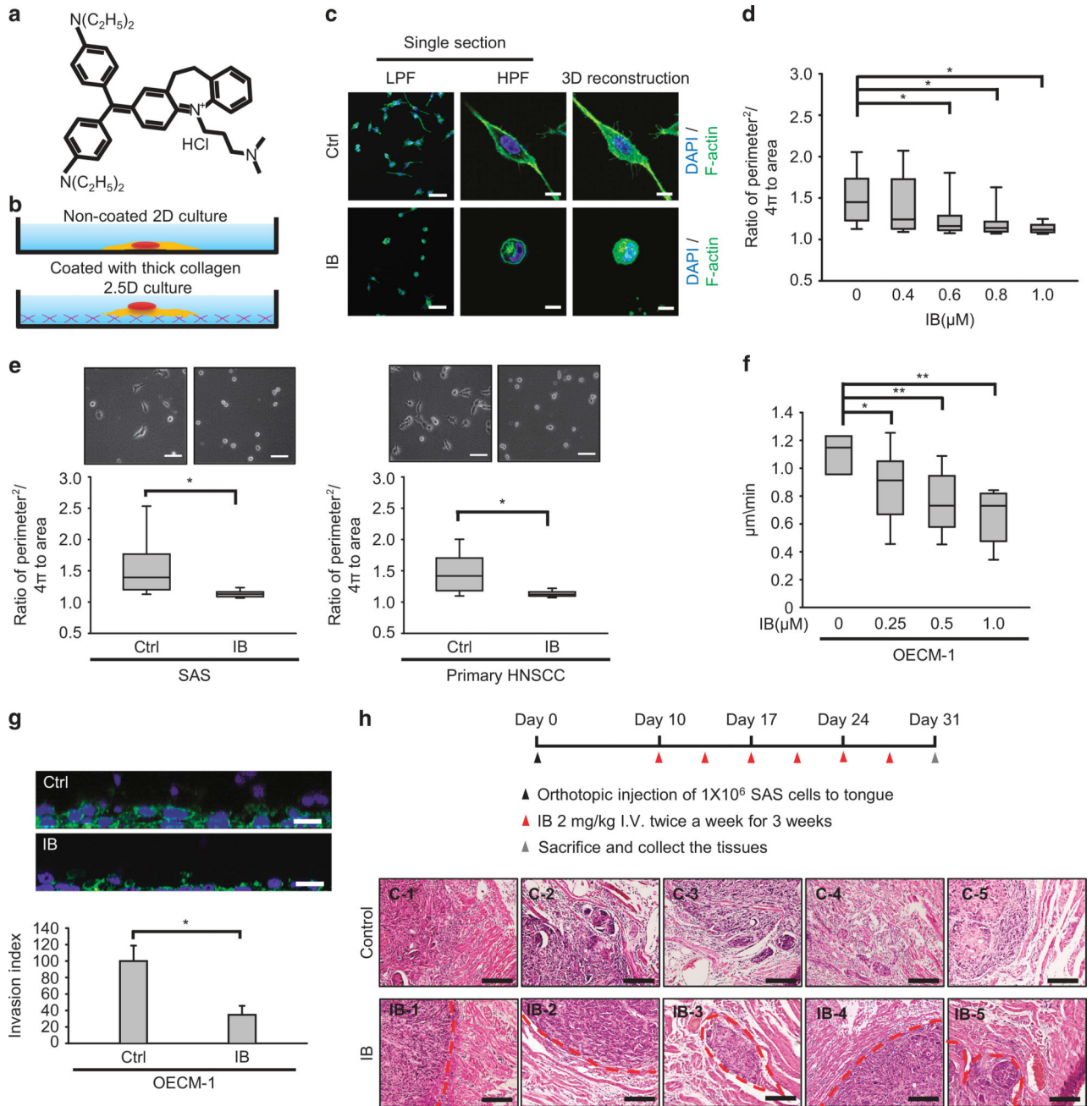
Figure 1.
Imipramine blue (IB) inhibits mesenchymal-mode movement and local invasion of head and neck cancer cells. (**a**) Chemical structure of IB. (**b**) The illustration for 2D culture (traditional cell culture on plastic dishes) and 2.5D culture (cultivation on top of the thick collagen). (**c**) Immunofluorescence to show the morphology and actin organization of OECM-1 cells treated with 1 μM IB for 24 h or a control vehicle (Ctrl) in 2.5D culture. The first and second rows are the single section with low-power field (LPF) and high-power field (HPF). The third row is the 3D reconstruction image. Green, F-actin; blue, nuclei. Scale bar =25 μm (first row), 10 μm (second and third rows). (**d**) The morphology index (ratio of

perimeter^2/4π to area) of OECM-1 cells cultured in 2.5D system under different concentrations of IB treatment for 24 h (n =150 for each concentration). *P< 0.01 by Student's t-test. (**e**, left) The representative phase-contrast images (upper) and morphology index (lower) of SAS cells treated with 1 μM IB or a control vehicle (Ctrl) for 24 h. (**e**, right) The representative phase-contrast images (upper) and morphology index (lower) of the primary HNSCC cells treated with 1 μM IB or a control vehicle (Ctrl) for 24 h; n=150 for each condition. *P< 0.01 by Student's t-test. (**f**) Quantification of motility speed of OECM-1 cells receiving different concentrations of IB treatment for 24 h and cultivated in 2.5D system; n=10 for each concentration. *P< 0.05, **P< 0.01 by Student's t-test. (**g**) 3D invasion assay. Upper: the representative images of OECM-1 cells invading into collagen after 1 μM IB or a control vehicle (Ctrl) treatment for 24 h. Scale bar=25 μm. Lower: the relative invasion index; n=3 for each condition. The result was normalized by the viability of cells in each condition. *P< 0.01 by Student's t-test. (**h**) Orthotopic implantation experiment for examining the invasive behaviour of orthotopic tumours treated with IB or a control vehicle. Upper: the schema of experiment. Lower: histological examination of the implanted sites of the nude mice treated with IB or a control vehicle (n=5 for each group). Each picture indicates the result of one mouse. IB-1 to IB-5 indicate the IB group, C-1 to C-5 indicate the control group. The red broken lines indicate the border between the implanted tumour and adjacent muscles. Scale bar =400 μm. The box plots in (**d**–**f**) represent sample maximum (upper end of whisker), upper quartile (top of box), median (band in the box), lower quartile (bottom of box), and sample minimum (lower end of whisker). The bar chart in (**g**) represents mean± s.e.m.
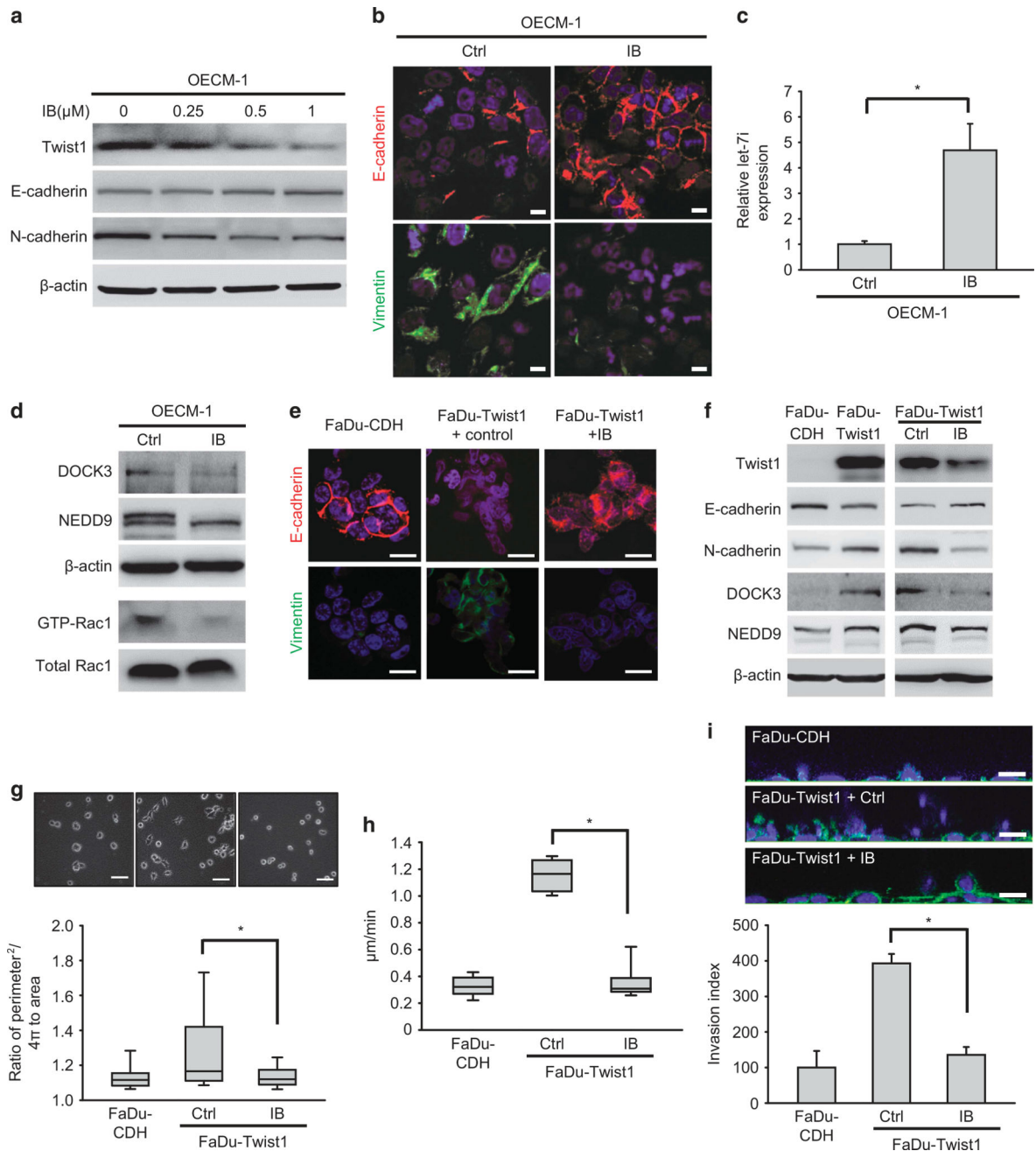
Figure 2.
IB represses Twist1-induced EMT and mesenchymal migration. (**a**) Western blot of Twist1, E-cadherin and N-cadherin in OECM-1 cells receiving different concentrations of IB treatment for 24 h. β-actin is a loading control. (**b**) Immunofluorescence of OECM-1 cells treated with 1 μM IB or a control vehicle (Ctrl) for 24 h. Scale bar=10 μm. Red, E-cadherin; green, vimentin; blue, nuclei. (**c**) Quantitative reverse transcription–PCR (RT–PCR) for examining the relative expression of let-7i in OECM-1 cells treated with 1 μM IB or a control vehicle (Ctrl) for 24 h (*n*=3). *P< 0.01 by Student's *t*-test. (**d**) Expression of GTP bound of Rac1, total Rac1, NEDD9 and DOCK3 in OECM-1 cells treated with 1 μM IB or a control

vehicle (Ctrl) for 24 h. Total Rac1 was applied as a control of activated Rac1, and β-actin was a loading control. (**e**) Immunofluorescence of FaDu cells transfected with a control vector (FaDu-CDH), a Twist1 expression vector (FaDu-Twist1) treated with 1 μM IB or a control vehicle for 24 h. Scale bar=20 μm. Red, E-cadherin; green, vimentin; blue, nuclei. (**f**) Western blot of Twist1, E-cadherin, N-cadherin, NEDD9 and DOCK3 in FaDu-CDH versus FaDu-Twist1 (left) and FaDu-Twist1 treated with 1 μM IB or a control vehicle (Ctrl)(right) for 24 h. β-actin is a loading control. (**g**) The representative phase-contrast images (upper) and morphology index (lower) of FaDu-CDH and FaDu-Twist1 treated with 1 μM IB or a control vehicle (Ctrl) for 24 h; n=150 for each condition. Scale bar=50 μm. *P< 0.01 by Student's t-test. (**h**) Quantification of motility speed of FaDu-CDH and FaDu-Twist1 treated with 1 μM IB or a control vehicle (Ctrl) for 24 h; n=10 for each concentration. *P< 0.01 by Student's t-test. (**i**) 3D invasion assay. Upper: the representative images of cells invading into collagen after 24 h in FaDu-CDH and FaDu-Twist1 treated with 1 μM IB or a control vehicle (Ctrl) for 24 h. The result was normalized by the viability of cells in each condition. Scale bar=25 μm. Lower: the relative invasion index; n=3 for each condition. *P< 0.01 by Student's t-test. The box plots in (**g** and **h**) represent sample maximum (upper end of whisker), upper quartile (top of box), median (band in the box), lower quartile (bottom of box), and sample minimum (lower end of whisker). The bar charts in (**c** and **i**) represent mean±s.e.m.
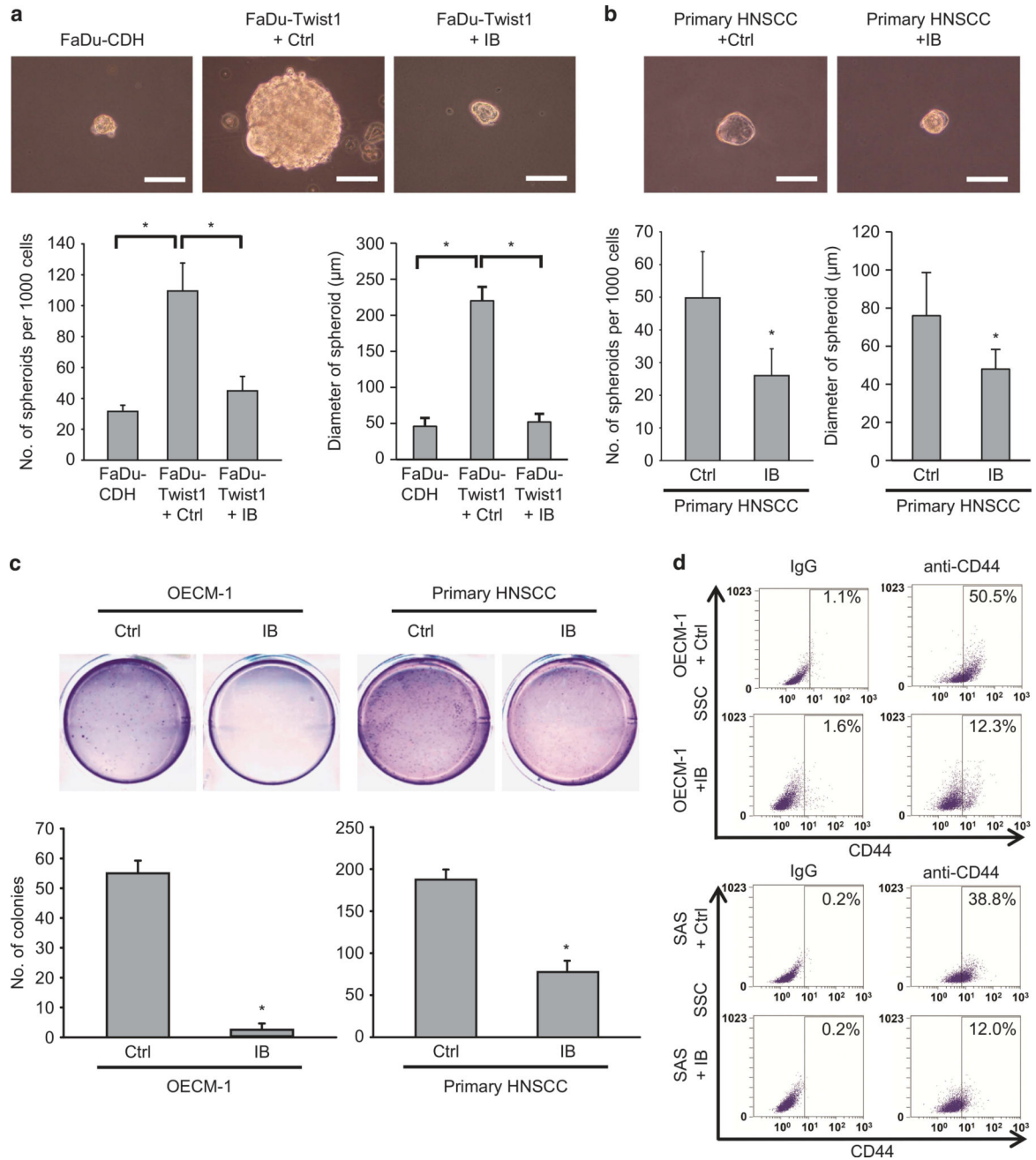
Figure 3.
IB suppressed stem-like properties of HNSCC cells. (**a**) Spheroid formation assay in FaDu-CDH and FaDu-Twist1 treated with 1 μM IB or a control vehicle (Ctrl) for 24 h. Upper: representative pictures. Scale bar =100 μm. Lower: quantification of spheroid formation (left) and spheroid diameter (right); n= 3 for each condition. $*P < 0.01$ by Student's t-test. (**b**) Spheroid formation assay in the primary HNSCC culture treated with 1 μM IB or a control vehicle (Ctrl) for 24 h. Upper: representative pictures. Scale bar =100 μm. Lower: quantification of spheroid formation (left) and spheroid diameter (right); n=3 for each condition. $*P < 0.01$ by Student's t-test. (**c**) Soft agar colony formation assay in OECM-1

cells (left) and the primary HNSCC cells (right) treated with 1 μM IB or a control vehicle (Ctrl) for 24 h (*n*=3). *P< 0.01 by Student's *t*-test. (**d**) Flow cytometry analysis of CD44 in OECM-1 cells (upper) or SAS cells (lower) treated with 1 μM IB or a control vehicle (Ctrl) for 24 h. The percentages of CD44+ cells are shown in the right upper quadrant of each panel. Isotype IgG was used as a control. The bar charts in (**a**–**c**) represent mean ±s.e.m.

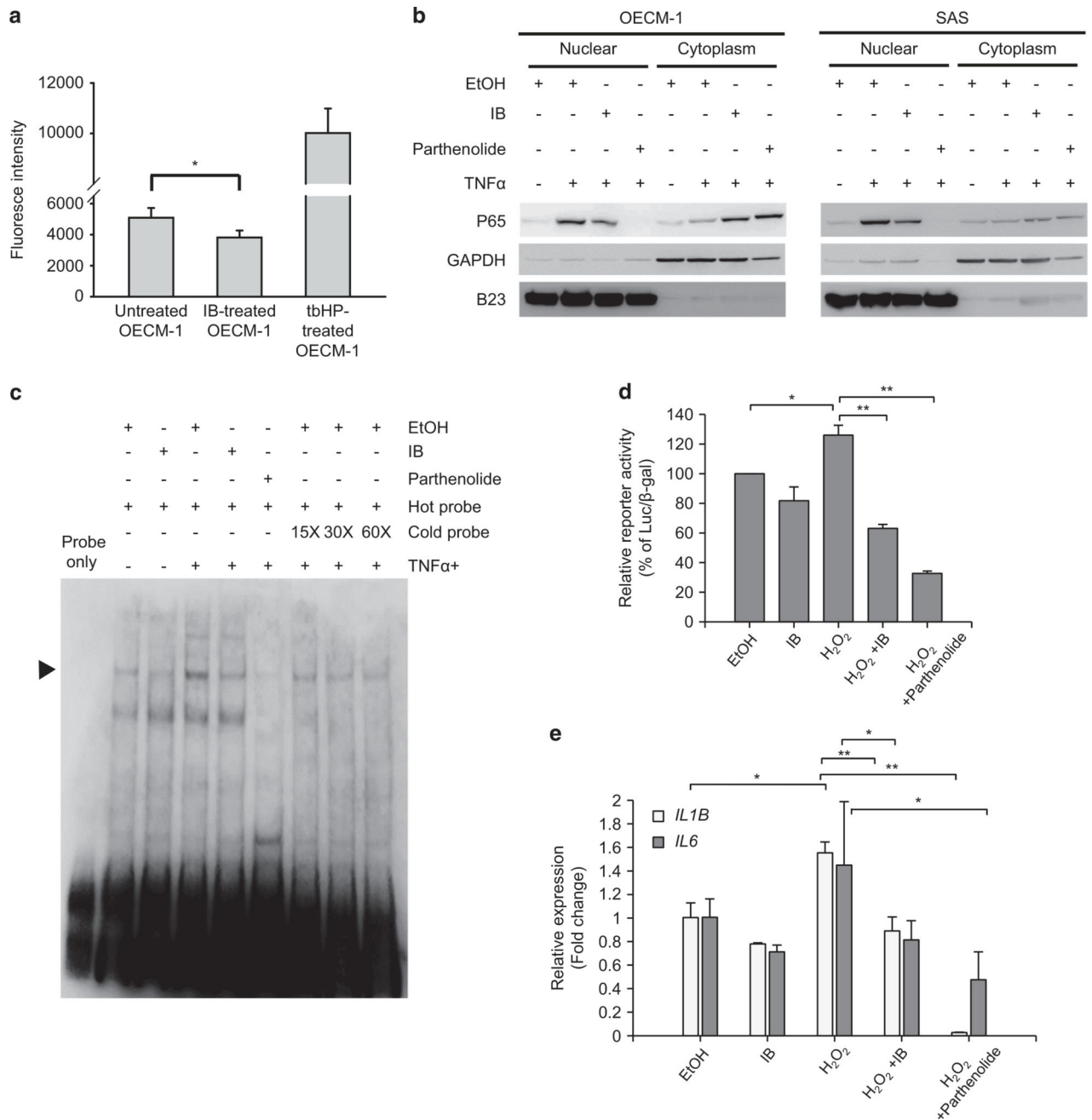**a**

b

c

d

e

Figure 4.
IB inactivates NF-κB pathway in HNSCC cells. (**a**) ROS detection assay in OECM-1 cells treated with 1 μM IB or a control vehicle (Ctrl) for 24 h. Treatment with 50 μM TBHP (*t*-butyl hydroperoxide) was a positive control of the experiment; *n*=3 for each condition. Data represent mean±s.e.m. *P< 0.05 by Student's *t*-test. (**b**) Western blot of nuclear and cytoplasmic p65 in OECM-1 cells (left) and SAS cells (right) treated with combination of different reagents. EtOH, the vehicle control; IB working concentration =1 μM for 24 h; TNFα, the positive control of the experiment, working concentration =20 ng/ml for 8 h; parthenolide, the NF-κB inhibitor as the negative control of the experiment, working

concentration =20 μM for 6 h. GADPH is the loading control for cytoplasmic proteins, whereas B23 is the loading control for nuclear proteins. (**c**) Electrophoretic mobility shift assay. The OECM-1 cells were treated with 20 ng/ml TNFα for 8 h for induction of NF-κB activation. The NF-κB activity of OECM-1 cells was detected by incubating the nuclear extracts with the biotin-labelled DNA probe containing the NF-κB binding sequence. IB working concentration =1 μM for 24 h; parthenolide working concentration =20 μM for 8 h. Different folds of unlabelled probes were used for competition assay. The arrow indicates the shifted band of NF-κB. (**d**) Luciferase reporter assay. The OECM-1 cells were co-transfected with the NF-κB reporter and pCMV-βgal and treated with different reagents as indicated. The relative reporter activity was presented as percentage of luciferase/β-gal compared with the control group. EtOH, the vehicle control; IB working concentration =1 μM for 24 h; H_2O_2 =80 μM for 24 h; parthenolide working concentration = 20 μM for 8 h; *n*=3 for each condition. *$P < 0.05$, **$P < 0.01$ by Student's *t*-test. (**e**) Reverse transcription and quantitative PCR (RT–qPCR) for detecting the expression of *IL1B* and *IL6* in OECM-1 cells receiving treatment of different reagents as indicated. EtOH, the vehicle control; IB working concentration =1 μM for 24 h; H_2O_2=80 μM for 24 h; parthenolide working concentration =20 μM for 8 h; *n* =3 for each condition. Data represent mean ±s.e.m. *$P < 0.05$, **$P < 0.01$ by Student's *t*-test.
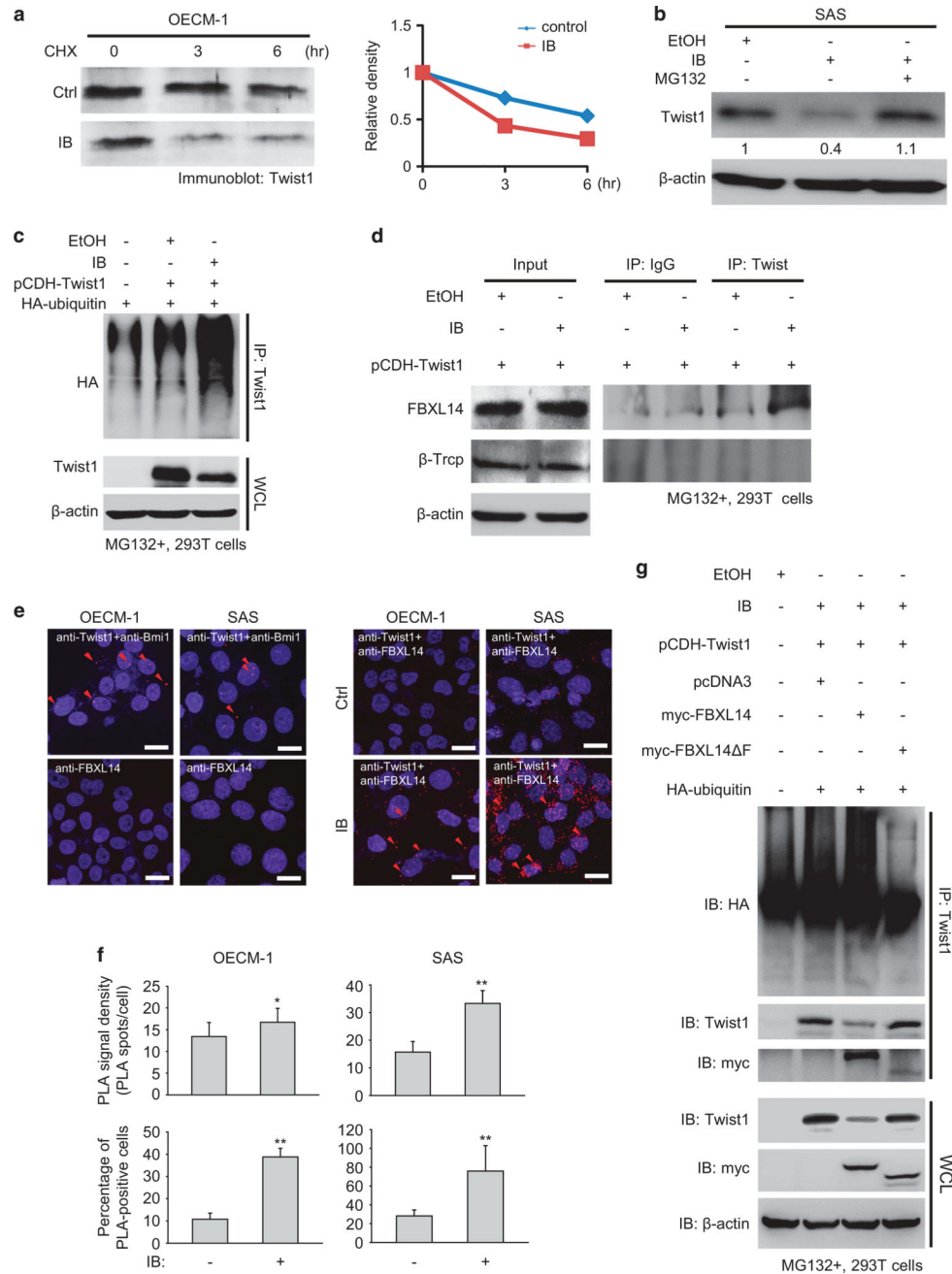
Figure 5.
IB promotes Twist1 polyubiquitination and degradation by enhancing the interaction between Twist1 and FBXL14. (**a**) Cycloheximide (CHX) pulse-chase assay. Left: western blot of Twist1 in OECM-1 cells treated with 1 μM IB or a control vehicle (Ctrl). CHX 50 μg/ml was added at indicated time points for inhibiting the *de novo* protein synthesis. Right: relative optical density of Twist1 at different time points. (**b**) Western blot of Twist1 in SAS cells treated with the indicated reagents. EtOH, the vehicle control; IB working concentration =1 μM; MG132, the proteasome inhibitor MG132 and the working concentration =20 μM. (**c**) Immunoprecipitation-western blot to show the polyubiquitinated

Twist1 in 293T cells under different transfection condition receiving 1 μM IB or a control vehicle treatment for 24 h. MG132 was added for stabilizing the polyubiquitinated Twist1. WCL, whole cell lysate. (**d**) Immunoprecipitation-western blot to show the interaction between Twist1 and the E3 ligases (FBXL14 and β-TrCP) in MG132-treated 293T cells receiving 1 μM IB or a control vehicle treatment for 24 h. Immunoglobulin G (IgG) was a control for immunoprecipitation. (**e**) The representative images of proximity ligation assay (PLA). The OECM-1 and SAS cells were treated with 1 μM IB or a control vehicle for 24 h, and then were incubated with the anti-FBXL14 and anti-Twist1 antibodies and detected by DuoLink probe (Olink Bioscience, Uppsala, Sweden). MG132 was added for stabilizing Twist1. The anti-Twist1 and anti-Bmi1 antibodies were used as a positive control. Scale bar =10 μm. The red dots indicate the positive PLA signal. The red arrows indicate the representative positive PLA signals. (**f**) Quantification of the PLA experiment. Upper panels: the PLA signal density (PLA dots/cell); lower panels: the percentage of PLA-positive cells; n=10 for each condition. Data represent mean ±s.e.m. *$P < 0.05$, **$P < 0.01$. (**g**) Immunoprecipitation-western blot of 293T cells under different transfection conditions and treated with 1 μM IB or a control vehicle for 24 h. WCL, whole cell lysate.
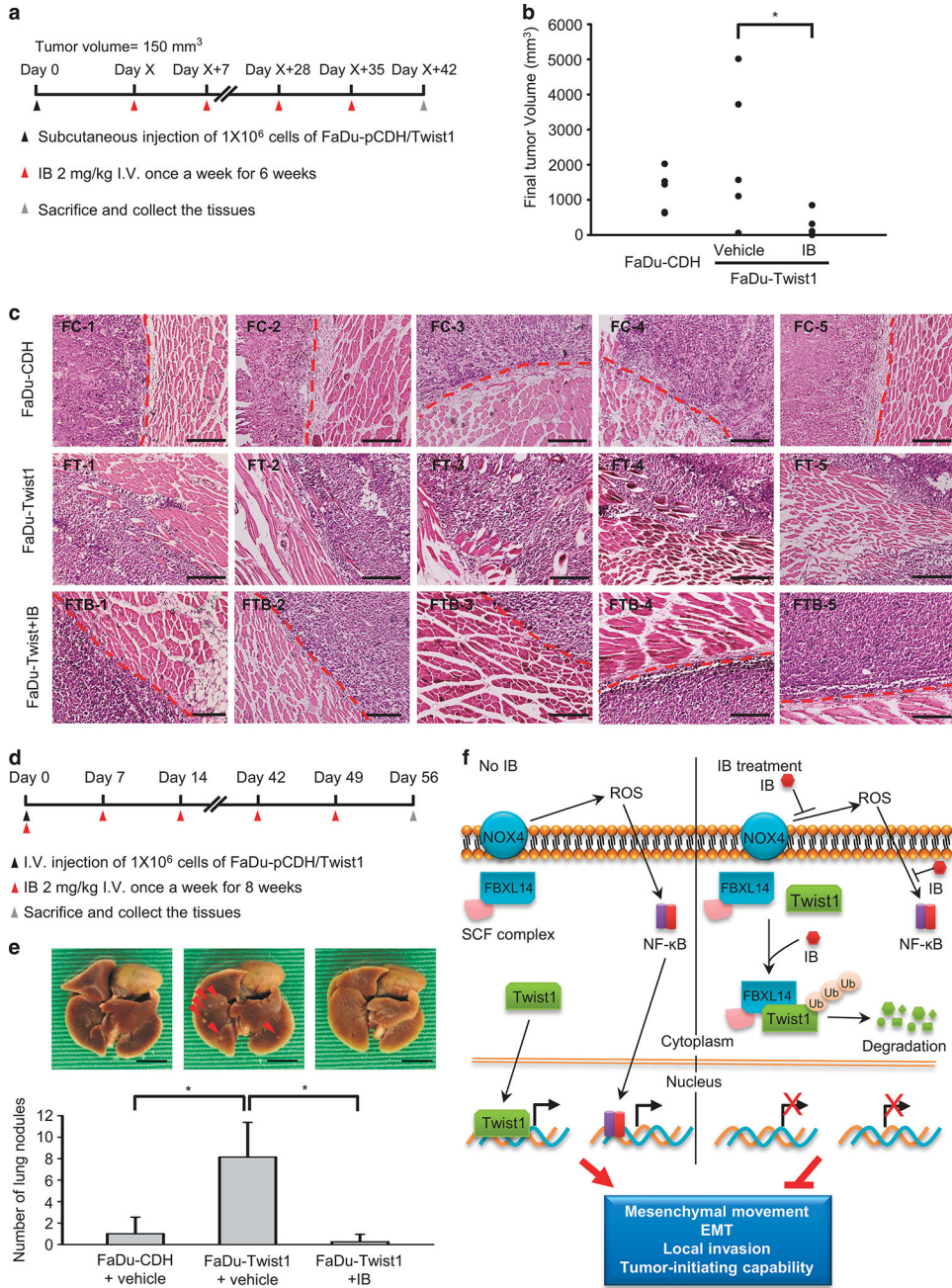
Figure 6.
IB represses HNSCC invasion *in vivo*. (**a**) Schema for the subcutaneous xenotransplantation experiment. (**b**) Illustration of the tumour volume of the mice receiving injection of FaDu-CDH or FaDu-Twist1 with IB or a control vehicle treatment; *n*=5 for each group. *$P < 0.05$ by Student's *t*-test. (**c**) Histological examination of the implanted sites of the nude mice receiving injection of FaDu-CDH (FC) or FaDu-Twist1 (FT), and FaDu-Twist1 treated with IB (FTB). Each picture indicates the result of one mouse. The red broken lines indicate the border between the implanted tumour and adjacent muscles. Scale bar= 400 μm. (**d**) Schema for the tail vein injection experiment. (**e**) Upper: the photos for showing the metastatic

nodules in mice receiving injection of FaDu-CDH and FaDu-Twist1, and treated with IB or a control vehicle. The red arrows indicate the representative metastatic nodules. Lower: Number of metastatic nodules counted in mice receiving injection of FaDu-CDH or FaDu-Twist1 with IB or a control vehicle treatment; n =5 for each group. *P < 0.05 by Student's t-test. (**f**) The model for illustrating the anti-invasive mechanisms of IB in HNSCC. IB treatment inactivates NF-κB signal by ROS generation and ROS-induced NF-κB activation, and IB promotes Twist1 degradation through FBXL14-mediated polyubiquitination. These events lead to the suppression of mesenchymal movement, EMT, local invasion and tumour initiation capability of HNSCC cells.